Infrared Light-Emitting Devices from Antenna-Coupled Luttinger Liquid Plasmons In Carbon Nanotubes

SeokJae Yoo, Sihan Zhao, and Feng Wang

Phys. Rev. Lett. **127**, 257702 — Published 14 December 2021

DOI: 10.1103/PhysRevLett.127.257702

Infrared light-emitting devices from antenna-coupled Luttinger liquid plasmons in carbon nanotubes

SeokJae Yoo[1,2], Sihan Zhao[1,3], and Feng Wang[1,4,5*]

[1] Department of Physics, University of California at Berkeley, Berkeley, CA, USA.

[2] Department of Physics, Inha University, Incheon, Korea.

[3] Interdisciplinary Center for Quantum Information, State Key Laboratory of Modern Optical Instrumentation, and Zhejiang Province Key Laboratory of Quantum Technology and Device, Department of Physics, Zhejiang University, Hangzhou, China

[4] Materials Science Division, Lawrence Berkeley National Laboratory, Berkeley, California, USA.

[5] Kavli Energy NanoSciences Institute at the University of California, Berkeley and the Lawrence Berkeley National Laboratory, Berkeley, California, USA.

Electrically driven light-emitting devices provide highly energy-efficient lighting at visible wavelengths, and they have transformed photonic and electronic lighting applications. Efficient infrared light-emitting devices, however, have been challenging because bandgap emission from semiconductors becomes inefficient in the mid- to far-infrared spectral range. Here we investigate infrared light-emitting devices (IRLEDs) based on Luttinger liquid (LL) plasmons in one-dimensional (1D) metallic carbon nanotubes. Elementary excitations in LL are characterized by collective charge and spin excitations, *i.e.* plasmons and spinons. Consequently, electrons injected into the nanotubes transform efficiently into LL plasmons, a hybrid excitation of electromagnetic fields and electrons. We design nanoantennas coupled to the carbon nanotube to radiate LL plasmons into the far-field. LL-based IRLEDs can be designed to selectively emit at wavelengths across the far- and mid-infrared spectra. An electrical-to-optical power conversion efficiency up to 3.2% may be achieved. Such efficient and narrowband LL-based IRLEDs can enable novel infrared nanophotonic applications.

Infrared light sources are important for a wide range of applications ranging from spectroscopy and molecular sensing to material processing because the infrared radiation interacts strongly with molecular vibration modes [1,2]. Efficient solid-state lighting, however, has been limited in the infrared spectral range, unlike its visible wavelength counterparts [1]. Solid-state infrared light-emitting devices (IRLEDs) have been explored using narrow-gap semiconducting materials such as III-V, II-VI, and lead-salt semiconductor alloys [1,3,4], but their bandgap emissions suffer from low quantum efficiency (<1%) because the non-radiative Auger process dominates the electron-hole recombination in narrow-gap semiconductors [5–10].

Rather than using narrow-gap semiconductors, we explore here IRLEDs based on a Luttinger liquid (LL), a strongly correlated electronic matter confined in one-dimensional (1D) metals with peculiar properties such as the spin-charge separation and the power-law decay of the

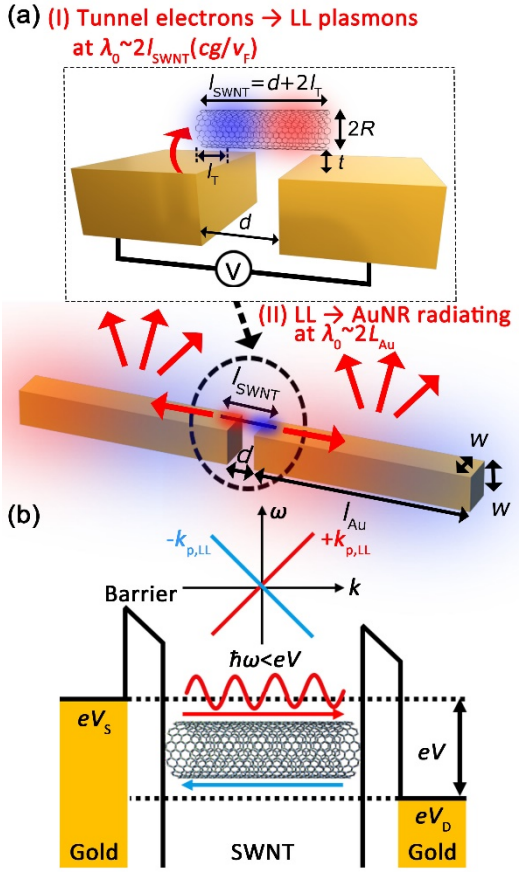

FIG. 1. (a) IRLED structure composed of SWNT and AuNR (l_{Au}: a length of AuNR, w: width of AuNR, d: AuNR gap size, t: a tunneling gap between SWNT and AuNR, l_T: an overlap length of SWNT and AuNR defining $l_{SWNT}=d+2l_T$). SWNT supports the Luttinger liquid (LL). Inset shows the dashed circle area near the AuNR gap. (b) A two-terminal geometry with the bias voltage $V=V_S-V_D$ and the linear LL dispersion (inset). The injected electrons are converted into the LL plasmons at the frequencies $\omega=(v_F/g)k_{p,LL}=2\pi c/\lambda_0 \leq eV/\hbar$.

correlation functions [11–15]. 1D LL does not have quasiparticle excitations, *e.g.* quasi-free electrons [11]. Instead, the elementary excitations of LL become plasmons and spinons, which are collective oscillations of charge and spin, respectively [16]. Once electrons are injected into LL, a substantial fraction of energy is directly converted to plasmons at finite frequencies. It enables efficient infrared lighting with electrically excited LL plasmons if the near-field plasmons can be coupled to the far-field. Many 1D metallic systems supports LL [12,17–21], but LL approximation in the 1D systems often breaks down for high energy excitations in the 1D systems due to the nonlinear dispersion. Contrastingly, single-walled carbon nanotubes (SWNTs) provide the linear dispersion up to ~1 eV, making them an ideal platform for the infrared LL plasmons [20–31], exhibiting the power-law scaling of the tunneling conductance [30,31], the shot noise currents [25,34,35], and high quality factor infrared plasmons [24,32,33].

We investigate theoretically high-efficiency IRLEDs using antenna-coupled LL plasmons in single-walled carbon nanotubes (SWNTs). We estimate a 14% injection efficiency to excite

infrared LL plasmons in SWNTs. We design a gold nanorod (AuNR) antenna to couple the deep-subwavelength LL plasmons to the far-field. It significantly mitigates the large wavelength mismatch between the LL plasmons and infrared photons and boosts the far-field radiation yield. Our calculation shows that an electrical-to-optical power conversion efficiency, *i.e.* the quantum efficiency, over 3.2% can be achieved. Such efficient IRLEDs based on 1D LL in SWNTs can enable a new type of infrared nanophotonic applications.

Figure 1a illustrates the AuNR-coupled SWNT IRLED (SWNT/AuNR IRLED). The metallic SWNT has l_{SWNT} and R=1 nm, which bridges the AuNR antennas with a gap of d. Each AuNR has l_{Au}=3.8 μm and W=60 nm, yielding an antenna resonance around λ_0=11 μm. This wavelength is in the middle of the infrared atmospheric window (λ_0=8~14 μm). Electrons can be injected into LL in SWNT via tunneling from AuNRs [30,31,36–38]. We assume air gap as a tunneling junction with t=1 nm and l_T=5 nm (Fig. 1a).

Light emission in our IRLED is achieved via two-step process (Fig. 1a). In step I, we inject electrons into SWNT by tunneling from biased AuNRs, resulting in the efficient generation of the LL plasmons in a two-terminal geometry [39,40]. The SWNT length l_{SWNT} in our IRLED is comparable to the LL plasmon wavelength $\lambda_{p,LL}$ to support the Fabry-Perot resonances (FPRs). In step II, AuNRs act as a nanoantenna converting the deep-subwavelength LL plasmons to the photons. We investigate the efficiency of each step and examine the quantum efficiency of our LL-based IRLEDs, characterizing the electrical-to-optical power conversion.

We first estimate the injection efficiency, characterizing the electrical-to-plasmonic power conversion, in step I. Using a LL theory [22], we calculate the tunneling density of states (TDOS) for electron tunneling at bias energy $\varepsilon=eV$ from a metallic electrode to LL. TDOS spectrum is composed of peaks of the quantum numbers of plasmons (n_p) and spinons (n_0), *i.e.* $A(\varepsilon)=\sum_{n_p,n_0\geq 0} A_{n_p n_0}(\varepsilon)=\sum_{n_p,n_0\geq 0} C_{n_p n_0}\delta\{E_C+n_p\varepsilon_p+(n_0+1/2)\varepsilon_0-\varepsilon\}$ with the spinon energy $\varepsilon_0=\pi\hbar v_F/L_{SWNT}$, the plasmon energy $\varepsilon_p=\varepsilon_0/g$, and the Coulomb energy $E_C=(\varepsilon_p^2-\varepsilon_0^2)/8\varepsilon_0$ [22]. $C_{n_p n_0}/C_{00}=c_{3/4}^{n_0}\sum_{0\leq i\leq j\leq n_p} c_{2g^{(+)}}^{n_p-1} c_{g^{(-)}}^{j-i} c_{g^{(-)}}^{i}$, determines a height of each TDOS peak, where $g^{(\pm)}\equiv(g^{-1}\pm g)/16$ and $c_g^n\equiv\Gamma(g+n)/\Gamma(g)\Gamma(1+n)$ with the Euler gamma function Γ. TDOS spectrum (Fig. 2a) shows multipole plasmon resonances; dipole, quadrupole, and octupole (n_p=1, 2, and 3, respectively), while peaks of n_p=0 are the ground state. Each plasmon accompany spinon resonances of $n_0\geq 0$. TDOS determines the current ($I(\varepsilon)$, Fig. S1a) and the power ($P(\varepsilon)$, Fig. S1b) of the tunnel electrons by $A(\varepsilon)\propto dI(\varepsilon)/d\varepsilon=d^2P(\varepsilon)/d\varepsilon^2$, where $I(\varepsilon)=\sum_{n_p,n_0\geq 0}\int_0^{\varepsilon} A_{n_p n_0}(\varepsilon')d\varepsilon'\equiv\sum_{n_p,n_0\geq 0} I_{n_p n_0}(\varepsilon)$ and $P(\varepsilon)=\sum_{n_p,n_0\geq 0}\int_0^{\varepsilon} I_{n_p n_0}(\varepsilon')d\varepsilon'\equiv\sum_{n_p,n_0\geq 0} P_{n_p n_0}(\varepsilon)$.

In the LL-based IRLEDs, the dipolar plasmon (n_p=1) alone contributes to the IR emission, while the higher plasmons ($n_p\neq 1$) and spinons ($n_p\neq 0$) are loss channels. The power of the

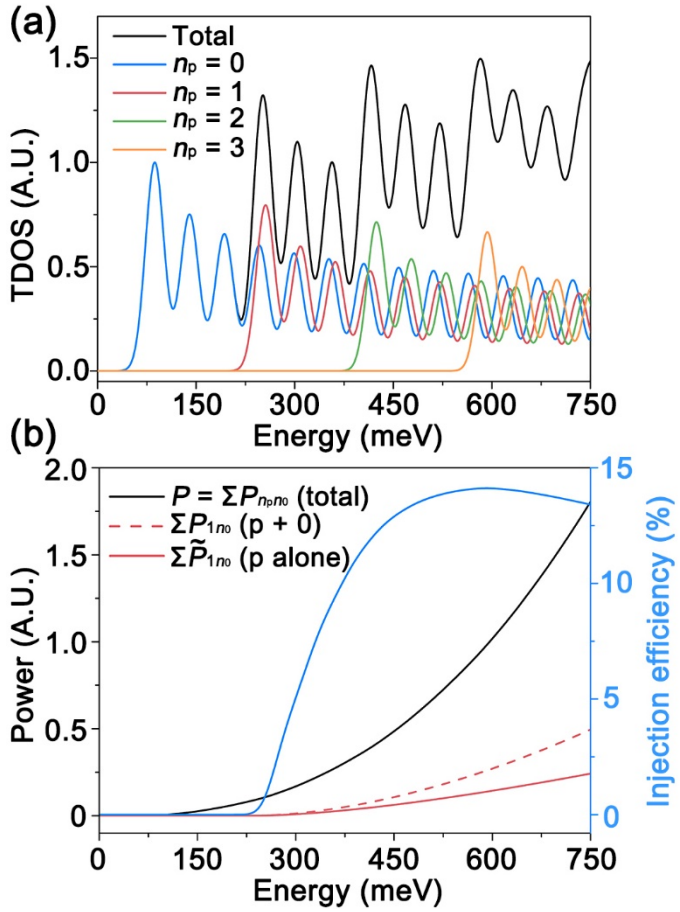

FIG. 2. (a) The tunneling density of states (TDOS) at the end of SWNT with g=0.31, R=1 nm, and l_{SWNT}=31.2 nm (black line). TDOS is decomposed into the plasmon (n_p) and spinon (n_0) modes (colored lines with ε_0=53.0 meV, ε_p=169 meV, E_C=60.5 meV, and the broadening of 20.0 meV). (b) Power spectra of the total LL ($P(\varepsilon) \equiv \sum_{n_p \geq 0, n_0 \geq 0} P_{n_p n_0}(\varepsilon)$ black line), the dipolar plasmons with the spinons ($\sum_{n_0 \geq 0} P_{1n_0}(\varepsilon)$ dashed red line), and the pure dipolar plasmons ($\sum_{n_0 \geq 0} \tilde{P}_{1n_0}(\varepsilon)$; red line). The injection efficiency of the dipolar plasmons ($\eta_{inj}(\varepsilon) \equiv \sum_{n_0 \geq 0} \tilde{P}_{1n_0}(\varepsilon) / P(\varepsilon)$ blue line).

dipolar plasmons can be calculated as $\sum_{n_0 \geq 0} \tilde{P}_{1n_0}(\varepsilon) \equiv \sum_{n_0 \geq 0} P_{1n_0}(\varepsilon) \left[\varepsilon_p / \left\{ \varepsilon_p + (n_0 + 1/2)\varepsilon_0 + E_C \right\} \right]$. We can define the injection efficiency as $\eta_{inj} \equiv \sum_{n_0 \geq 0} \tilde{P}_{1n_0}(\varepsilon) / P(\varepsilon)$. Fig. 2b shows η_{inj} can be achieved up to 14% at 590 meV, and it is significantly higher than the injection efficiency of narrow-gap LEDs (<1%) [5–10] and the inelastic tunneling efficiency through a metallic gap (~10^{-6}/eV) [41].

To evaluate the radiation efficiency in step II, we perform electromagnetic calculations for

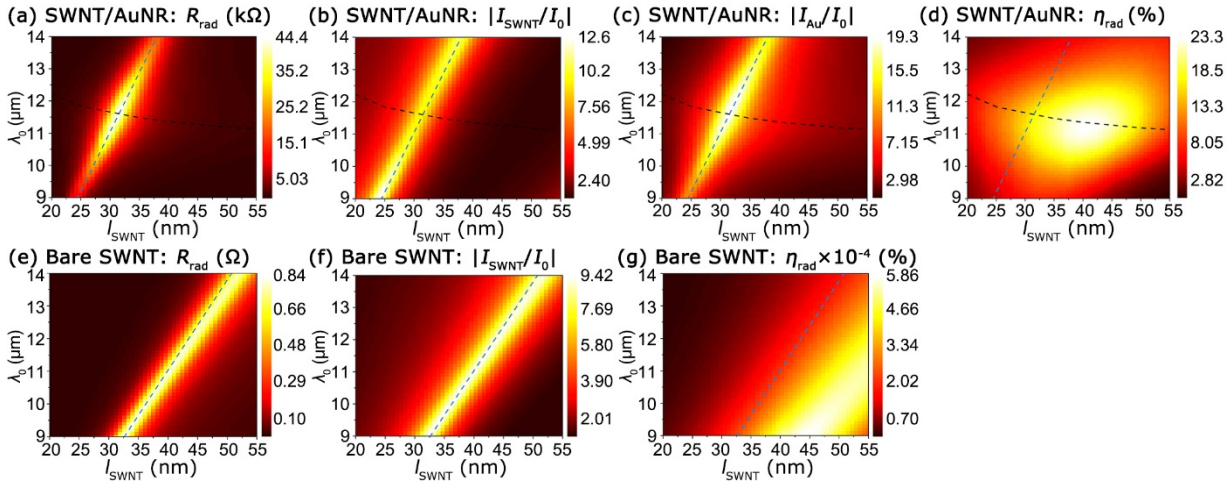

FIG. 3. (a) The radiation resistance $R_{rad}\equiv 2P_{rad}/I_0^2$, (b) the current $|I_{SWNT}/I_0|$ of SWNT, (c) the current $|I_{Au}/I_0|$ of AuNRs, and (d) the radiation efficiency $\eta_{rad}\equiv P_{rad}/(P_{rad}+P_{\Omega,Au}+P_{\Omega,SWNT})$ of the SWNT/AuNR IRLEDs with the radiation power P_{rad}, the gold absorption power $P_{\Omega,Au}$, and the SWNT absorption power $P_{\Omega,SWNT}$ upon the current source I_0 in SWNT. Black and blue dashed lines are AuNR and SWNT FPRs, respectively. (e) The radiation resistance R_{rad}, (f) the current $|I_{SWNT}/I_0|$, and (g) the radiation efficiency $\eta_{rad}=P_{rad}/(P_{rad}+ P_{\Omega,SWNT})$ of bare SWNTs.

our IRLEDs. We model SWNT as a metallic cylinder with a radius of R and the permittivity of ε_{SWNT}. By correlating a LL theory with an electromagnetic theory, we can express ε_{SWNT} as (see Supplemental Material for the derivation):

$$\mathrm{Re}\left\{\varepsilon_{SWNT}(\omega)\right\} = -\frac{16}{1-g^2}\frac{k_e e^2}{\varepsilon_{eff}\hbar v_F}\frac{v_F^2}{\pi R^2}\frac{1}{\omega^2}, \quad (1)$$

with $k_e=1/4\pi\varepsilon_0$ and the reduced Plank constant $\hbar$. We find ε_{SWNT} can be written in terms of g and R. $\mathrm{Im}(\varepsilon_{SWNT})$ can be obtained by $Q=\left\{\omega\mathrm{Re}\left(d\varepsilon_{SWNT}/d\omega\right)\right\}/\left\{2\,\mathrm{Im}\left(\varepsilon_{SWNT}\right)\right\}$ [42]. Hereinafter, we use experimental values [24,32], g=0.3 and Q=20.

In Fig. 3 we compare the radiation properties of a bare SWNT and our SWNT/AuNR IRLEDs. As shown in Fig. 3a, the radiation resistance $R_{rad}\equiv 2P_{rad}/I_0^2$ is determined by the spectral proximity of SWNT FPR (blue line) and AuNR FPR (black line). Inheriting the linearity of LL plasmon dispersion (Fig. 1b), the SWNT FPR follows a linear FPR dispersion, $\lambda_0 = 2l_{SWNT}\left(cg/v_F\right)/\left(1-\varphi_{SWNT}/\pi\right)$ with φ_{SWNT}/π~0.36 [43,44]. The AuNR FPR is almost constant over l_{SWNT} changes due to the AuNR FPR condition $\lambda_0 = 2l_{Au}/\left(1-\varphi_{Au}/\pi\right)$. The maximum radiation resistance R_{rad}~44.4 kΩ appears at the crossing point of two modes, namely, the maximum radiation point, *i.e.* (l_{SWNT}, λ_0)=(31 nm, 12 μm). Contrastingly, the bare SWNT in Fig. 3e shows poor R_{rad}, originating from the wavelength mismatch.

Figure 3 also shows the optical currents,

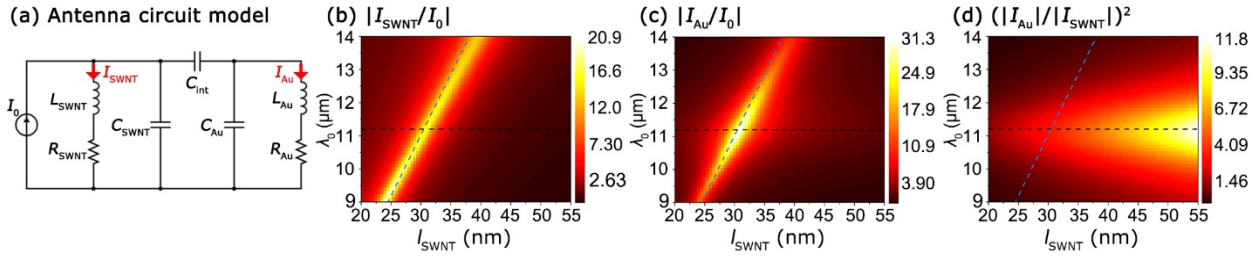

FIG. 4. (a) The antenna circuit model consists of two RLC circuits with the resistance R, inductance L, and capacitance C. C_{int} connects two RLC circuits characterized by the resonant impedances $Z_{SWNT}(\omega)$ and $Z_{Au}(\omega)$, respectively. Model results of (b) $|I_{SWNT}/I_0|$, (c) $|I_{Au}/I_0|$, and (d) $(|I_{Au}|/|I_{SWNT}|)^2$ (Black and blue dashed lines: FPR modes of AuNR and SWNT, respectively.)

$\left|I_{Au(SWNT)}\right| \equiv (\text{area}/\text{length})\int_{V_{Au(SWNT)}} dV \left|-i\omega\left(\varepsilon_{Au(SWNT)}-\varepsilon_0\right)\mathbf{E}\right|$, in SWNT and AuNR [45]. They s how FPR modes of SWNT and AuNR (Figs. 3b, c, and f). In Figs. 3b&c, we find that $|I_{Au}/I_0|$ i s maximized, while $|I_{SWNT}/I_0|$ slightly decreases when two FPRs meet. This implies AuNRs ta ke the current from SWNT to radiate the LL plasmons to the far-field. Comparing R_{rad} (Fig. 3a) and $|I_{Au}/I_0|$ (Fig. 3c), we can find that they exhibit the same pat tern. This shows that AuNRs play a dominant role in the far-field radiation in our IRLEDs.

Figures 3d&g compare the radiation efficiency η_{rad} of our SWNT/AuNR IRLED and the bare SWNT. We define η_{rad} as $\eta_{rad} \equiv P_{rad}/P_{tot} = \left(2P_{rad}/\left|I_{Au}\right|^2\right)/\left\{\left(2P_{rad}/\left|I_{Au}\right|^2\right)+R_{\Omega,Au}+\left(\left|I_{SWNT}\right|/\left|I_{Au}\right|\right)^2 R_{\Omega,SWNT}\right\}$ with the total power $P_{tot}\equiv P_{rad}+P_{\Omega,Au}+P_{\Omega,SWNT}$, the absorption power of SWNT (AuNR) $P_{\Omega,SWNT(Au)}=|I_{SWNT(Au)}|^2 R_{\Omega,SWNT(Au)}/2$, and the Ohmic resistance of SWNT (Au) $R_{\Omega,SWNT(Au)}=(\text{length}/\text{area})\text{Im}\{1/\omega\varepsilon_0(1-\varepsilon_{SWNT(Au)})\}$ (Fig. S2c&d). η_{rad} of the bare SWNT (Fig. 3g) is poor because of the wavelength mismatch. SWNT/AuNR IRLED (Fig. 3f) has higher η_{rad} with the enhancement along AuNR FPR. The maximum efficiency point with η_{rad}=23% appears at (l_{SWNT}, λ_0)=(40 nm, 11 μm) away from the maximum radiation point at (31 nm, 12 μm) with η_{rad}=17%. The resultant quantum efficiencies at the two points reach $\eta_Q=\eta_{inj}\times\eta_{rad}\sim$3.2% and 2.4%, respectively. These are higher than other light sources using the mid-infrared bandgap emission, whose quantum efficiencies are limited to <1% [1,8–10].

To understand the emission properties, we develop a circuit model shown in Fig. 4a (see Supplemental Material for details). It consists of two parallel RLC circuits describing the resonances in SWNT and AuNRs, respectively. Two RLC circuits are capacitively coupled through the interaction capacitance C_{int}. The antenna impedance, $Z_{SWNT(Au)}(\omega) = i\omega L_{SWNT(Au)}\left(\omega_{0,SWNT(Au)}^2/\omega^2\right)\left\{\left(\omega^2+i\gamma_{SWNT(Au)}\omega\right)/\left(\omega^2-\omega_{0,SWNT(Au)}^2+i\gamma_{SWNT(Au)}\omega\right)\right\}$ characterizes each RLC circuit, and it includes the resonance information of SWNT (AuNR) with $\omega_{0,SWNT(Au)} \equiv \sqrt{1/L_{SWNT(Au)}C_{SWNT(Au)}}$ and $\gamma_{SWNT(Au)} \equiv R_{SWNT(Au)}/L_{SWNT(Au)}$. Solving the antenna circuit in Fig. 4a, we can obtain I_{SWNT} and I_{Au} (Figs. 4b&c) that reproduce Figs. 3b&c.

Fig. 4a also explains η_{rad} in Fig 3d. In η_{rad}, the ratio $(|I_{SWNT}|/|I_{Au}|)^2$ (Fig. S2a) is responsible for η_{rad} because $(2P_{rad}/|I_{Au}|^2)$, $R_{\Omega,Au}$, and $R_{\Omega,SWNT}$ (Figs. S2b-d) do not show η_{rad} behavior in Fig. 3d. We obtain

$$\left(\left|I_{Au}\right|/\left|I_{SWNT}\right|\right)^2=\left(L_{SWNT}/L_{Au}\right)^2\left\{\left(\omega^2+\gamma_{SWNT}^2\right)/\left(\omega^2+\gamma_{Au}^2\right)\right\}\left|Z_{Au}\left(\omega\right)\right|^2/\left|1/i\omega C_{\text{int}}+Z_{Au}\left(\omega\right)\right|^2$$

from Fig. 4a. Fig. 4d shows that $(|I_{\text{Au}}|/|I_{\text{SWNT}}|)^2$ is enhanced at the AuNR FPR not at the SWNT FPR because it does not have $Z_{\text{SWNT}}(\omega)$. It also has $(L_{\text{SWNT}})^2 \propto (l_{\text{SWNT}})^2$, explaining why the maximum efficiency point (Fig. 3d) differs from the maximum radiation point (Fig. 3a).

In conclusion, we suggested IRLED based on antenna-coupled LL plasmons. Our IRLED can operate with the quantum efficiency of more than 3.2% with the combination of the highly efficient LL plasmon excitation and nanoantenna. Further improvement of the IRLED efficiency can be achieved by further optimization of the nanoantenna design and a semiconducting injection electrode. Also, our scheme can be applied to a broad spectral range from terahertz to near-infrared frequencies where the emission wavelength can be tuned by geometry of SWNT and AuNR lengths.

This work was funded by the U.S. Department of Energy, Office of Science, Office of Basic Energy Sciences, Materials Sciences and Engineering Division under Contract No. DE-AC02-05-CH11231 (sp2-Bonded Materials Program KC2207). SeokJae Yoo was supported by the National Research Foundation of Korea (NRF) grants funded by the Ministry of Education (NRF-2017R1A6A3A11034238) and the Ministry of Science and ICT (NRF-2019R1A4A1028121 and CAMM-2014M3A6B3063710). Sihan Zhao was supported by ZJU 100 Talents Program (107200*1942221R3).

* Corresponding author. fengwang76@berkeley.edu

[1] D. Jung, S. Bank, M. L. Lee, and D. Wasserman, *Next-Generation Mid-Infrared Sources*, J. Opt. **19**, 123001 (2017).

[2] J. Biegert, P. K. Bates, and O. Chalus, *New Mid-Infrared Light Sources*, IEEE J. Sel. Top. Quantum Electron. **18**, 531 (2012).

[3] T. C. McGill and D. A. Collins, *Prospects for the Future of Narrow Bandgap Materials*, Semicond. Sci. Technol. **8**, S1 (1993).

[4] M. Tonouchi, *Cutting-Edge Terahertz Technology*, Nat. Photonics **1**, 97 (2007).

[5] Y. Aytac, B. V. Olson, J. K. Kim, E. A. Shaner, S. D. Hawkins, J. F. Klem, J. Olesberg, M. E. Flatté, and T. F. Boggess, *Bandgap and Temperature Dependence of Auger Recombination in InAs/InAsSb Type-II Superlattices*, J. Appl. Phys. **119**, 215705 (2016).

[6] H. P. Hjalmarson and S. R. Kurtz, *Electron Auger Processes in Mid-infrared InAsSb/InGaAs Heterostructures*, Appl. Phys. Lett. **69**, 949 (1996).

[7] B. Vinter, *Auger Recombination in Narrow-Gap Semiconductor Superlattices*, Phys. Rev. B **66**, 045324 (2002).

[8] R. J. Ricker, S. R. Provence, D. T. Norton, T. F. Boggess, and J. P. Prineas, *Broadband Mid-Infrared Superlattice Light-Emitting Diodes*, J. Appl. Phys. **121**, 185701 (2017).

[9] E. J. Koerperick, D. T. Norton, J. T. Olesberg, B. V. Olson, J. P. Prineas, and T. F. Boggess, *Cascaded Superlattice InAs/GaSb Light-Emitting Diodes for Operation in the Long-Wave Infrared*, IEEE J. Quantum Electron. **47**, 50 (2011).

[10] A. Krier, M. Stone, Q. D. Zhuang, P.-W. Liu, G. Tsai, and H. H. Lin, *Mid-Infrared Electroluminescence at Room Temperature from InAsSb Multi-Quantum-Well Light-Emitting Diodes*, Appl. Phys. Lett. **89**, 091110 (2006).

[11] H. J. Schulz, G. Cuniberti, and P. Pieri, *Fermi Liquids and Luttinger Liquids*, in *Field Theories for Low-Dimensional Condensed Matter Systems* (2000), pp. 9–81.

[12] A. M. Chang, *Chiral Luttinger Liquids at the Fractional Quantum Hall Edge*, Rev. Mod. Phys. **75**, 1449 (2003).

[13] M. P. A. Fisher and L. I. Glazman, *Transport in a One-Dimensional Luttinger Liquid*, in *Mesoscopic Electron Transport* (Springer Netherlands, Dordrecht, 1997), pp. 331–

373.

[14] T. L. Schmidt, A. Imambekov, and L. I. Glazman, *Spin-Charge Separation in One-Dimensional Fermion Systems beyond Luttinger Liquid Theory*, Phys. Rev. B **82**, 245104 (2010).

[15] A. Imambekov, T. L. Schmidt, and L. I. Glazman, *One-Dimensional Quantum Liquids: Beyond the Luttinger Liquid Paradigm*, Rev. Mod. Phys. **84**, 1253 (2012).

[16] M. P. A. Fisher and L. I. Glazman, *Transport in a One-Dimensional Luttinger Liquid*, in *Mesoscopic Electron Transport* (Springer Netherlands, Dordrecht, 1997), pp. 331–373.

[17] W. Jolie, C. Murray, P. S. Weiß, J. Hall, F. Portner, N. Atodiresei, A. V. Krasheninnikov, C. Busse, H. P. Komsa, A. Rosch, and T. Michely, *Tomonaga-Luttinger Liquid in a Box: Electrons Confined within MoS2 Mirror-Twin Boundaries*, Phys. Rev. X **9**, 11055 (2019).

[18] J. Wang, J. Niu, B. Shao, G. Yang, C. Lu, M. Li, Z. Zhou, X. Chuai, J. Chen, N. Lu, B. Huang, Y. Wang, L. Li, and M. Liu, *A Tied Fermi Liquid to Luttinger Liquid Model for Nonlinear Transport in Conducting Polymers*, Nat. Commun. **12**, 1 (2021).

[19] C. Blumenstein, J. Schäfer, S. Mietke, S. Meyer, A. Dollinger, M. Lochner, X. Y. Cui, L. Patthey, R. Matzdorf, and R. Claessen, *Atomically Controlled Quantum Chains Hosting a Tomonaga-Luttinger Liquid*, Nat. Phys. **7**, 776 (2011).

[20] X. L. Qi and S. C. Zhang, *Topological Insulators and Superconductors*, Rev. Mod. Phys. **83**, (2011).

[21] A. M. Chang, L. N. Pfeiffer, and K. W. West, *Observation of Chiral Luttinger Behavior in Electron Tunneling into Fractional Quantum Hall Edges*, Phys. Rev. Lett. **77**, 2538 (1996).

[22] C. Kane, L. Balents, and M. Fisher, *Coulomb Interactions and Mesoscopic Effects in Carbon Nanotubes*, Phys. Rev. Lett. **79**, 5086 (1997).

[23] R. Egger and A. O. Gogolin, *Effective Low-Energy Theory for Correlated Carbon Nanotubes*, Phys. Rev. Lett. **79**, 5082 (1997).

[24] S. Zhao, S. Wang, F. Wu, W. Shi, I. B. Utama, T. Lyu, L. Jiang, Y. Su, S. Wang, K. Watanabe, T. Taniguchi, A. Zettl, X. Zhang, C. Zhou, and F. Wang, *Correlation of Electron Tunneling and Plasmon Propagation in a Luttinger Liquid*, Phys. Rev. Lett. **121**, 047702 (2018).

[25] N. Y. Kim, P. Recher, W. D. Oliver, Y. Yamamoto, J. Kong, and H. Dai, *Tomonaga-Luttinger Liquid Features in Ballistic Single-Walled Carbon Nanotubes: Conductance and Shot Noise*, Phys. Rev. Lett. **99**, 036802 (2007).

[26] B. Gao, A. Komnik, R. Egger, D. C. Glattli, and A. Bachtold, *Evidence for Luttinger-Liquid Behavior in Crossed Metallic Single-Wall Nanotubes*, Phys. Rev. Lett. **92**, 216804 (2004).

[27] R. Saito, G. Dresselhaus, and M. S. Dresselhaus, *Physical Properties of Carbon Nanotubes* (Imperial College Press, London, 1998).

[28] J. Lee, S. Eggert, H. Kim, S.-J. Kahng, H. Shinohara, and Y. Kuk, *Real Space Imaging of One-Dimensional Standing Waves: Direct Evidence for a Luttinger Liquid*, Phys.

Rev. Lett. **93**, 166403 (2004).

[29] J. Nygard, D. H. Cobden, M. Bockrath, P. L. McEuen, and P. E. Lindelof, *Electrical Transport Measurements on Single-Walled Carbon Nanotubes*, Appl. Phys. A Mater. Sci. Process. **69**, 297 (1999).

[30] M. Bockrath, D. H. Cobden, J. Lu, A. G. Rinzler, R. E. Smalley, L. Balents, and P. L. McEuen, *Luttinger-Liquid Behaviour in Carbon Nanotubes*, Nature **397**, 598 (1999).

[31] Z. Yao, H. W. C. Postma, L. Balents, and C. Dekker, *Carbon Nanotube Intramolecular Junctions*, Nature **402**, 273 (1999).

[32] Z. Shi, X. Hong, H. A. Bechtel, B. Zeng, M. C. Martin, K. Watanabe, T. Taniguchi, Y.-R. Shen, and F. Wang, *Observation of a Luttinger-Liquid Plasmon in Metallic Single-Walled Carbon Nanotubes*, Nat. Photonics **9**, 515 (2015).

[33] S. Wang, F. Wu, S. Zhao, K. Watanabe, T. Taniguchi, C. Zhou, and F. Wang, *Logarithm Diameter Scaling and Carrier Density Independence of One-Dimensional Luttinger Liquid Plasmon*, Nano Lett. **19**, 2360 (2019).

[34] P. Recher, N. Y. Kim, and Y. Yamamoto, *Tomonaga-Luttinger Liquid Correlations and Fabry-Perot Interference in Conductance and Finite-Frequency Shot Noise in a Single-Walled Carbon Nanotube*, Phys. Rev. B **74**, 235438 (2006).

[35] S. Pugnetti, F. Dolcini, D. Bercioux, and H. Grabert, *Electron Tunneling into a Quantum Wire in the Fabry-Pérot Regime*, Phys. Rev. B **79**, 035121 (2009).

[36] M. S. Fuhrer, J. Nygård, L. Shih, F. M., Y.-G. Yoon, M. S. C. Mazzoni, H. J. Choi, J. Ihm, S. G. Louie, A. Zettl, and P. L. McEuen, *Crossed Nanotube Junctions*, Science (80-.). **288**, 494 (2000).

[37] M. Bockrath, *Single-Electron Transport in Ropes of Carbon Nanotubes*, Science (80-.). **275**, 1922 (1997).

[38] S. Zhao, S. Yoo, S. Wang, B. Lyu, S. Kahn, F. Wu, Z. Zhao, D. Cui, W. Zhao, Y. Yoon, M. I. B. Utama, W. Shi, K. Watanabe, T. Taniguchi, M. F. Crommie, Z. Shi, C. Zhou, and F. Wang, *Tunneling Spectroscopy in Carbon Nanotube-Hexagonal Boron Nitride-Carbon Nanotube Heterojunctions*, Nano Lett. **20**, 6712 (2020).

[39] K.-V. Pham, F. Piéchon, K.-I. Imura, and P. Lederer, *Tomonaga-Luttinger Liquid with Reservoirs in a Multiterminal Geometry*, Phys. Rev. B **68**, 205110 (2003).

[40] K.-I. Imura, K.-V. Pham, P. Lederer, and F. Piéchon, *Conductance of One-Dimensional Quantum Wires*, Phys. Rev. B **66**, 035313 (2002).

[41] M. Parzefall and L. Novotny, *Optical Antennas Driven by Quantum Tunneling: A Key Issues Review*, Reports Prog. Phys. **82**, 112401 (2019).

[42] F. Wang and Y. Shen, *General Properties of Local Plasmons in Metal Nanostructures*, Phys. Rev. Lett. **97**, 1 (2006).

[43] J.-H. H. Kang, S. Wang, Z. Shi, W. Zhao, E. Yablonovitch, and F. Wang, *Goos-Hänchen Shift and Even–Odd Peak Oscillations in Edge-Reflections of Surface Polaritons in Atomically Thin Crystals*, Nano Lett. **17**, 1768 (2017).

[44] X. Luo, C. Hu, B. Lyu, L. Yang, X. Zhou, A. Deng, J.-H. Kang, and Z. Shi, *Reflection Phase Shift of One-Dimensional Plasmon Polaritons in Carbon Nanotubes*, Phys. Rev. B **101**, 041407 (2020).

[45] D. Hone, B. Mühlschlegel, and D. J. Scalapino, *Theory of Light Emission from Small Particle Tunnel Junctions*, Appl. Phys. Lett. **33**, 203 (1978).

[46] S. Wang, S. Zhao, Z. Shi, F. Wu, Z. Zhao, L. Jiang, K. Watanabe, T. Taniguchi, A. Zettl, C. Zhou, and F. Wang, *Nonlinear Luttinger Liquid Plasmons in Semiconducting Single-Walled Carbon Nanotubes*, Nat. Mater. **19**, 986 (2020).

[47] X. Wei, T. Tanaka, Y. Yomogida, N. Sato, R. Saito, and H. Kataura, *Experimental Determination of Excitonic Band Structures of Single-Walled Carbon Nanotubes Using Circular Dichroism Spectra*, Nat. Commun. **7**, 12899 (2016).

[48] G. Hills, C. Lau, A. Wright, S. Fuller, M. D. Bishop, T. Srimani, P. Kanhaiya, R. Ho, A. Amer, Y. Stein, D. Murphy, Arvind, A. Chandrakasan, and M. M. Shulaker, *Modern Microprocessor Built from Complementary Carbon Nanotube Transistors*, Nature **572**, 595 (2019).

[49] J. Kern, R. Kullock, J. Prangsma, M. Emmerling, M. Kamp, and B. Hecht, *Electrically Driven Optical Antennas*, Nat. Photonics **9**, 582 (2015).

[50] J. C. Prangsma, J. Kern, A. G. Knapp, S. Grossmann, M. Emmerling, M. Kamp, and B. Hecht, *Electrically Connected Resonant Optical Antennas*, Nano Lett. **12**, 3915 (2012).

[51] E. D. Minot, Y. Yaish, V. Sazonova, J.-Y. Park, M. Brink, and P. L. McEuen, *Tuning Carbon Nanotube Band Gaps with Strain*, Phys. Rev. Lett. **90**, 156401 (2003).

[52] D. K. Gramotnev, A. Pors, M. Willatzen, and S. I. Bozhevolnyi, *Gap-Plasmon Nanoantennas and Bowtie Resonators*, Phys. Rev. B - Condens. Matter Mater. Phys. **85**, 1 (2012).

[53] H. Fischer and O. J. F. Martin, *Engineering the Optical Response of Plasmonic Nanoantennas*, Opt. Express **16**, 9144 (2008).

[54] B. Auguié and W. L. Barnes, *Collective Resonances in Gold Nanoparticle Arrays*, Phys. Rev. Lett. **101**, 1 (2008).

[55] M. S. Eggleston, K. Messer, L. Zhang, E. Yablonovitch, and M. C. Wu, *Optical Antenna Enhanced Spontaneous Emission*, Proc. Natl. Acad. Sci. **112**, 1704 (2015).

[56] R. L. Olmon, B. Slovick, T. W. Johnson, D. Shelton, S.-H. Oh, G. D. Boreman, and M. B. Raschke, *Optical Dielectric Function of Gold*, Phys. Rev. B **86**, 235147 (2012).

[57] M. Staffaroni, J. Conway, S. Vedantam, J. Tang, and E. Yablonovitch, *Circuit Analysis in Metal-Optics*, Photonics Nanostructures - Fundam. Appl. **10**, 166 (2012).

[58] A. Stratton, *Electromagnetic Theory* (Adams Press, 2008).

[59] A. T. de Hoop and G. de Jong, *Power Reciprocity in Antenna Theory*, Proc. Inst. Electr. Eng. **121**, 1051 (1974).